Available online at www.sciencedirect.com
SCIENCE DIRECT
Polymer 46 (2005) 8128–8140
polymer
www.elsevier.com/locate/polymer

The properties of poly(tetrafluoroethylene) (PTFE) in tension

P.J. Rae*, E.N. Brown

Los Alamos National Laboratory, Structure Property Relations, MST-8, MS-G755, Los Alamos, NM 85745, USA

Received 22 March 2005; received in revised form 16 June 2005; accepted 29 June 2005

Abstract

Samples of DuPont 7A and 7C Teflon (PTFE, poly(tetrafluoroethylene)) were tested in tension at strain-rates between 2×10^{-4} and 0.1 s^{-1} and temperatures between −50 and 150 °C. Additionally, using a Hopkinson bar, a temperature series was undertaken in tension between −50 and 23 °C at a strain rate of 800 s^{-1}. To investigate the small-strain response, strain gauges were used to measure axial and transverse strain allowing the Poisson ratio to be calculated. The effect of crystallinity was investigated using 7C material thermally processed to produce more amorphous material. As expected, the tensile mechanical properties of PTFE are significantly affected by strain-rate and temperature, but only to a limited extent by crystallinity. The Poisson ratio at small strains was found to differ in tension ($\approx$0.36) and compression ($\approx$0.46). Failure behavior and microstructure were correlated to temperature induced phase transitions.

Keywords: Polytetrafluoroethylene; PTFE; Tension

1. Introduction

The results presented here are a continuation of a multi-disciplinary effort aimed at understanding the mechanical response of a well characterized polymer both from a experimental view point and coupled with producing a robust theoretical model capable of being implemented into computer codes. A previous paper discussed the material characterization and properties found for PTFE in compression [1]. In this paper, the tensile properties under differing strain-rates and temperatures are presented. Additionally, the room temperature small-strain response ($\varepsilon<0.02$) will be presented.

Some previous data on the tensile properties of PTFE have been published. The earliest report found was by Renfrew in 1946 who tabulated a few mechanical parameters [2]. In common with most data collected on polymers material characterization is lacking. Additional data was published by Doban [3] who investigated the temperature effect from −40 to 350 °C and Thomas [4] who tabulates tensile properties vs. crystallinity. Doban also subjected samples to immersion in many common solvents for 24 h prior to testing, no change in tensile properties was noted. Samples heated to 300 °C for 1 month prior to testing showed a 10–20% drop in ultimate tensile stress. Joyce [5] measured the stress–strain behavior of PTFE 7C (of unreported processing or crystallinity) up to yield at −73, −18, and 21 °C for a range of crosshead rates. Fischer and Brown investigated the effects of temperature, rate and environment on the tensile behavior of PTFE [6,7] and showed that the tensile strength of PTFE is significantly decreased when in direct contact with liquid nitrogen. Sauer and Pae [8] reported that application of hydrostatic pressure up to 552 MPa serves to increase the yield stress and Young's modulus of PTFE, which was later modelled by Zerilli and Armstrong [9]. Tervoort et al. [10] investigated the tensile properties of a melt-processable PTFE that exhibited necking. Kletschkowski et al. [11] presented the tensile behavior of filled PTFE up to yield in connection with developing models for seal materials. Several authors have reported a reduction in the post-yield tensile behavior of PTFE following exposure to various types of radiation [12–15].

Nishioka made a brief study of the tensile properties of PTFE above the melt temperature [16] whilst Dyment measured some low-temperature properties from +20 to −196 °C [17]. The validity of the strain to failure in Dyment's research is cast in doubt by the work of Fischer

* Corresponding author. Tel.: +1 505 667 4436.
E-mail address: prae@lanl.gov (P.J. Rae).

0032-3861/$ - see front matter © 2005 Elsevier Ltd. All rights reserved.
doi:10.1016/j.polymer.2005.06.120

Table 1
Measured mass fraction crystallinities of the PTFE materials by different methods

Material	Density (kg m^{-3})	IR (%xstal)	Density (%xstal)	MDSC (%xstal)	WAXS (%xstal)
7A Teflon	2157.7 ± 0.1[a] 2158.3 ± 0.1[b]	73 ± 10	48 ± 1	38 ± 1	69 ± 2
7C Teflon	2168.9 ± 0.1[a] 2169.6 ± 0.1[b]	N/A	53 ± 1	38 ± 1	69 ± 2

[a] Pycnometry.
[b] Immersion.

[6] who studied the effect of immersion in cryogenic liquids on tensile properties of PTFE and found that only liquid helium did not alter the large-strain response.

A little data on the tensile response of Teflon as a function of temperature and under tensile creep conditions is presented in a DuPont publication [18], but the test conditions are inadequately explained and there is no material pedigree given. By far the best examination of the tensile response of PTFE was undertaken by Koo [19–21]. In Koo's PhD thesis, a vast amount of research into the ICI (Imperial Chemical Industries) PTFE product G-80 is presented. Both high and low crystallinity material was produced by differing the thermal history and the effect of temperature and strain-rate investigated. Creep data was obtained over a wide range of conditions. Sadly the strain component of the stress/strain data is suspect owing to the limitations of the system used. Dog-bone samples were cut and placed between gripping jaws.

The gauge length was established by the jaw separation and some correction for the material expansion or contraction was made. Unfortunately, the sample will inevitably have drawn to some degree from inside the grips. Since the strain was calculated from the crosshead displacement, a systematic error was produced that varies in magnitude with temperature. Despite this limitation and the age of the study, it remains the most extensive data available.

2. Materials

Billets 600 × 600 × 65 mm^3 of poly(tetrafluoroethylene) were prepared by Balfor Industries according to the ASTM standard ASTM-D-4894-98a by sintering and pressing poly(tetrafluoroethylene) molding powders (DuPont PTFE 7A and DuPont PTFE 7C). A full discussion of the material and the methods used to characterize it is given by Rae [1], but a brief overview will be presented for completeness.

PTFE is a complex material. It exhibits pressure and temperature generated phase transitions, is semi-crystalline and is insoluble in all common solvents [22]. Three relaxations with respect to temperature have been documented [23]. Being chemically inert makes characterization difficult. Methods have been postulated to estimate crystallinity [24–27], molecular weight [28–30] and crystallographic morphology [31–38], but to the authors knowledge, nothing is known about the amorphous orientation, or lack of, or the transition zone between crystalline and amorphous regions. It is therefore probable that pure PTFE is a three component composite of crystalline, amorphous and quasi-ordered materials.

The crystallinity of our 7A and 7C material was using several techniques [1] and the results are shown in Table 1. Both Refs. [1,39] contain arithmetic mistakes in the crystallinity calculated from density. The figures shown here are correct.

2.1. Thermally treated 7C material

The crystalline percentage of PTFE may be altered for a given molecular weight by altering the heat treatment profile used in production (thermal history) [4]. In order to understand some of the results generated, production of some PTFE with a different level of crystallinity was useful. It was found that thermally treating 7C Teflon produced a 3–4% wider variation in crystallinity than 7A and so this material was exclusively used for production of samples used in this study.

Bars of 7C 14 × 12 × 65 mm^3 were rough sawn for processing. Lower crystallinity material was produced by rapid ambient air cooling after a 5 h soak at 380 °C. Experiments with more rapid cooling produced inhomogeneous material that was not suitable for machining into test specimens. MDSC analysis to estimate the crystallinity was undertaken and found to be 26 ± 1% (cf. 38 ± 1% for the 7C material discussed elsewhere in this paper).

3. Experimental

Given the ductile nature of PTFE, the mechanical properties were investigated both at large and small strains. For this reason, all strains given in this paper are true-strains (logarithmic strains) unless otherwise stated. Additionally, a constant true strain-rate was utilized for all the large-strain experiments. The feedback loop from the testing machines was run closed loop to correctly speed up the crosshead as the samples deformed. In large-strain experiments, true-stress was calculated assuming a constant sample volume. This volume assumption has been shown to be true for strains greater than approximately 5% [1]. Samples were machined to form ASTM D-638 Type V specimens.

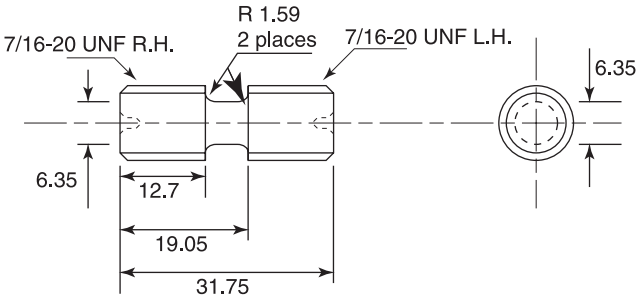

Fig. 1. Tensile Hopkinson bar specimen used for PTFE. Dimensions in mm.

At room temperature PTFE has a large strain to failure (500–600% engineering strain). Measuring these large displacements accurately is challenging. The method chosen for this study was a Messphysik ME-46 video extensometer. This device uses a black and white CCD camera to digitally capture as a function of time an image of the deforming sample, upon which fiducial markers have been attached. Using a sophisticated real-time correlation algorithm, the distance between the markers can be continuously measured. In this way, a non-contacting measurement of strain can be made to large values ($>1000\%$). Several methods of attaching fiducial markers were tried. The use of small sticky labels with a printed high-contrast white to black transition had been used previously but was found wanting on PTFE. The labels did not adhere adequately to the surface, particularly at high or low temperature. Additionally, because the label has a finite height, the strain under the label may cause it to peel at a random location. If the top and bottom marker remain attached at different locations the actual sample gauge length effectively alters during the test. The most effective method tried was to use wires held in place by small rubber 'O'-rings. By back-lighting the sample, a high contrast image about the wires was created and whilst the 'O'-rings deformed with the sample, the wires did not slip. At high or low temperatures (>50 or $<0\,^{\circ}C$) the 'O'-rings were unsatisfactory and small metal springs were used. The ME-46 is equipped with an analogue voltage output that is proportional to the measured strain. This voltage was fed into the testing machine, correctly scaled, and used to close the feedback crosshead-rate loop. The Young's modulus was determined from the initial tangent modulus and the yield stress was calculated with a 2% offset.

For the variable temperature experiments, a screw driven Instron 4482 frame was used. This machine has been fitted with a modern PC control system (MTS Testworks 4[1]) allowing a wide range of control modes and input channels. For the variable strain-rate tests, a MTS 810 servo-hydraulic machine was used. This machine runs MTS TestStar software allowing for full control over the test profile. All samples were allowed to equilibrate at the testing temperature for between 45 and 100 min prior to tensile testing.

The majority of samples were strained to failure. However, the small-strain response was also of interest. The video extensometer is not suitable for small strains (<0.02) and so strain gauges were bonded to 7A and 7C samples to obtain low-strain data. Normally, adhesives do not effectively adhere to PTFE. However, the surface of the samples was etched with a sodium based commercial product by ABB Etching[2], Arizona, USA. This results in surface removal of fluorine atoms and the subsequent replacement with OH groups when exposed to water vapour in the atmosphere. After etching, strain-gauge quality cyano-acrylate adhesive could be used to bond Measurements Group, USA, CEA-06-062WT-120 gauges to rectangular samples $80\times25\times4\,mm^3$. The strain gauges were bonded to the centre of the sample, well away from the grips used to load it. The gauges have two perpendicular active directions allowing axial and transverse strain to be recorded simultaneously. In this way, the Poisson ratio at small strains could be calculated.

3.1. Hopkinson bar experiments

High strain-rate data for 7C material was collected using the LANL tensile Hopkinson bar based on the design principles discussed by Nemat-Nasser [40] and further reviewed by Gray [41]. Owing to the low sound speeds in PTFE[3] and its low yield stress, collection of valid true-stress data was difficult. The magnitude of the transmitted stress was very low. For this reason, an atypical set-up was used. The incident bar was 250 maraging steel with traditional foil strain gauges, whilst the output bar was Ti-6Al-4V titanium with Micron Instruments SS-080-050-500P semiconductor gauges. Corrections to the data reduction software were made to account for differing bar impedances and wave-speeds and the gauges were calibrated at room temperature. The use of the lower impedance titanium output bar transmitted approximately twice the strain of a maraging steel bar. Semiconductor strain gauges have a nominal gauge factor of 150 compared with ≈2.1 for foil gauges. Therefore, coupled to an Ectron Corporation strain gauge amplifier, only an amplification gain of 50 was required to obtain useable signal levels with low noise. The gauge factor of semiconductor gauges is slightly sensitive to the magnitude of the imposed strain. Corrections to the signals were made for this.

Sample design proved challenging owing to the long ring-up time in PTFE. Fig. 1 shows the final geometry used. The ends of the Hopkinson bars are fitted with opposing direction threads in which the sample bottomed out. The

[1] www.mts.com.

[2] www.abbetch.com.

[3] Longitudinal sound speed $1333\pm3\,m\,s^{-1}$, shear sound speed $506\pm2\,m\,s^{-1}$ [1].

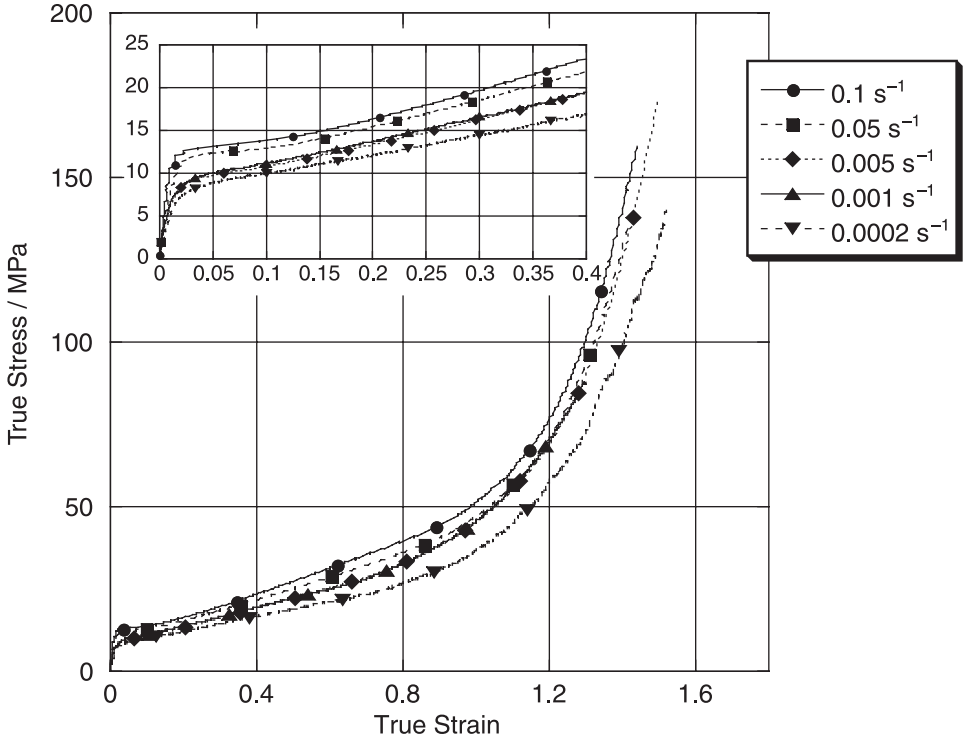

Fig. 2. Strain-rate response of 7A material. All tests undertaken at 23±1 °C.

gauge length is kept short to reduce ring-up time. For valid data to be collected in the Hopkinson bar, the assumption that the transmitted and reflected pulse instantaneously equals the incident pulse must be true. Even using the geometry described, this was not true until ≈10% true strain. For this reason, all data prior to this strain were excluded. Specimens were tested at three temperatures, 23, −15 and −50 °C. Colder samples were prepared by

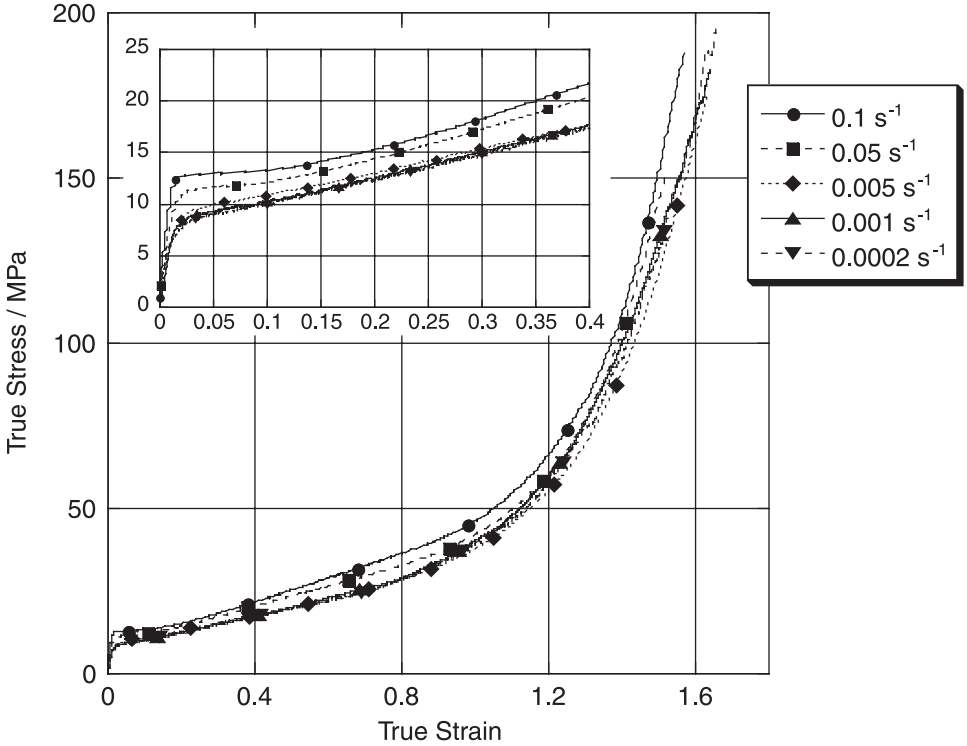

Fig. 3. Strain-rate response of 7C material. All tests undertaken at 23±1 °C.

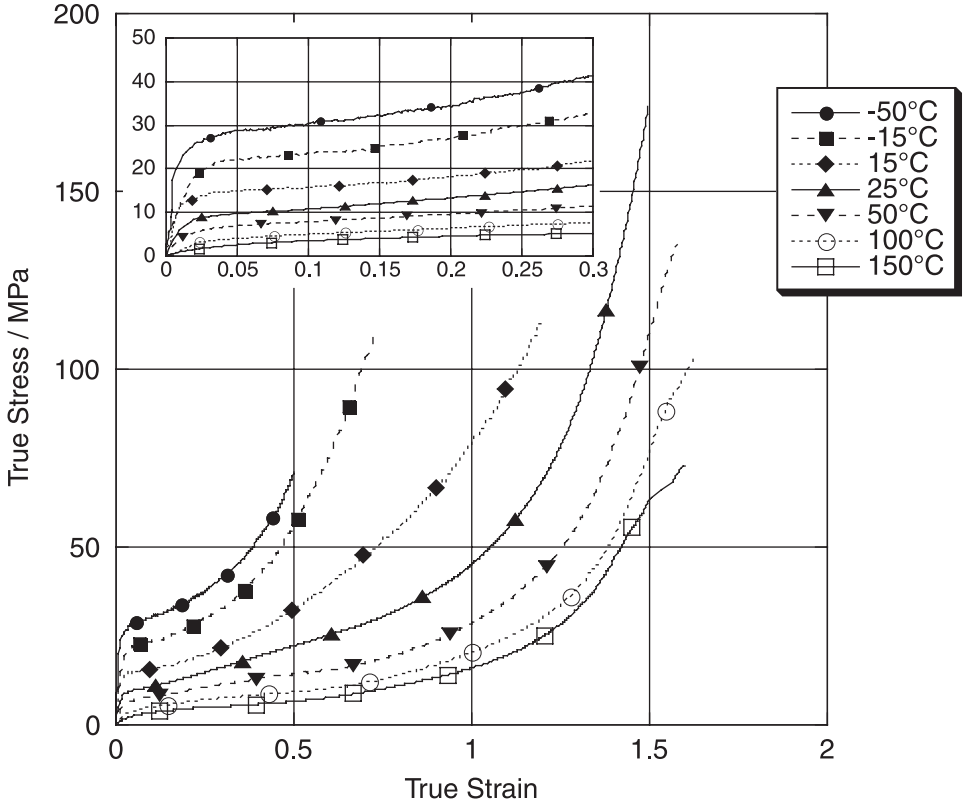

Fig. 4. Temperature sensitivity of 7A material. Strain-rate $5\times10^{-3}\ s^{-1}$.

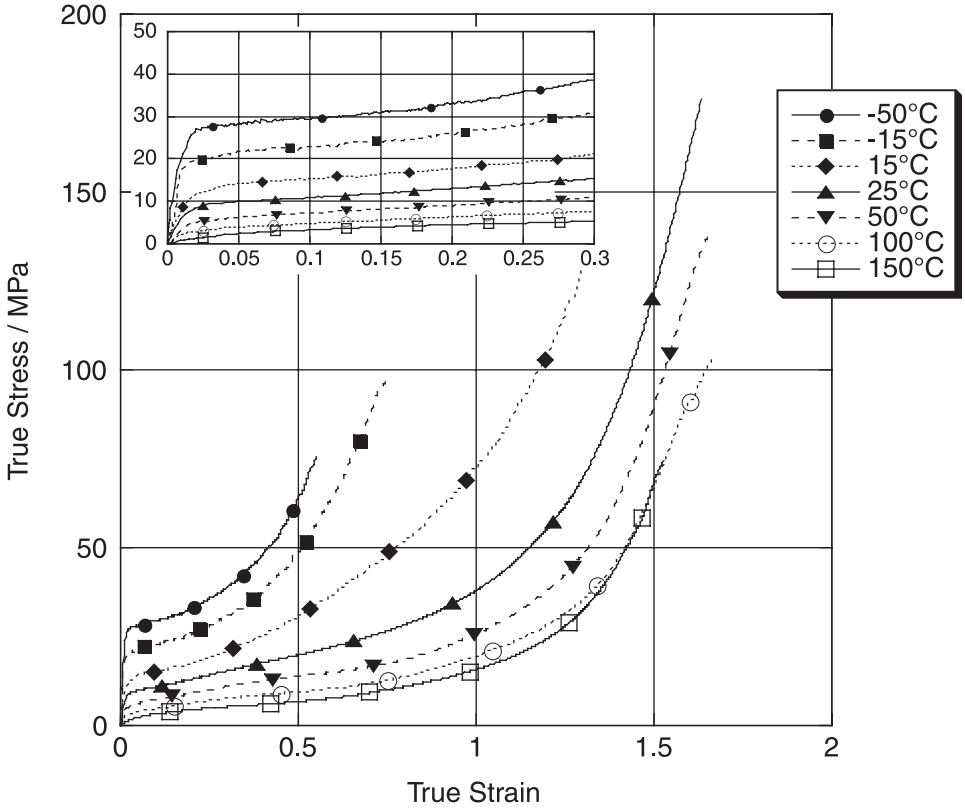

Fig. 5. Temperature sensitivity of 7C material. Strain-rate $5\times10^{-3}\ s^{-1}$.

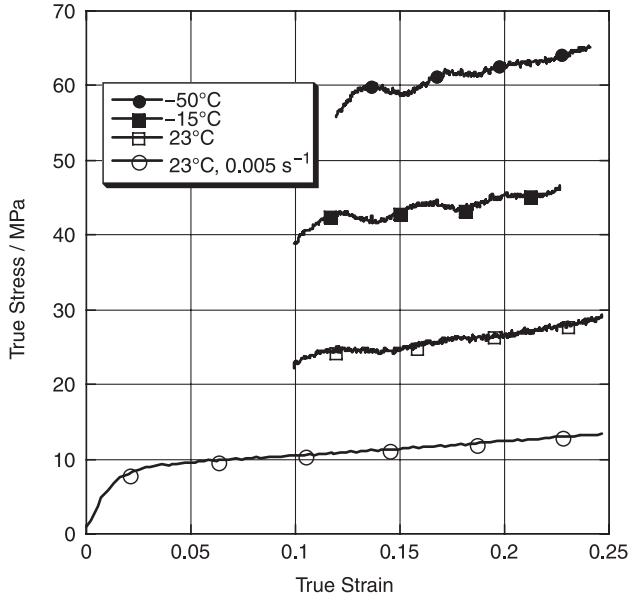

Fig. 6. High strain-rate response of 7C material vs. temperature. Strain-rate $800 \pm 70\ s^{-1}$.

blowing evaporating gas from liquid nitrogen over the samples until 5 s before conducting the test. The strain gauges are situated far enough from the sample location that the room temperature calibration is always valid.

3.2. Microscopy

Failure surface morphologies of the fractured samples were examined with a JEOL JSM-6300FXV scanning electron microscope (SEM). Following tensile failure, areas of interests were dissected, mounted on a conductive stage, and deposited with ≈75 Å of carbon. A Gatan 682 precision etch coating system with a rocking-rotational stage was used during deposition to impart uniform coating on porous microstructures. Carbon paint was applied from the sides of the samples to the stage to ensure optimal conductivity while taking care not to disturb the area of interest. Micrographs were obtained using 5 keV secondary electrons. Specimens prepared following this protocol generally showed little charging in the SEM and were free from beam damage.

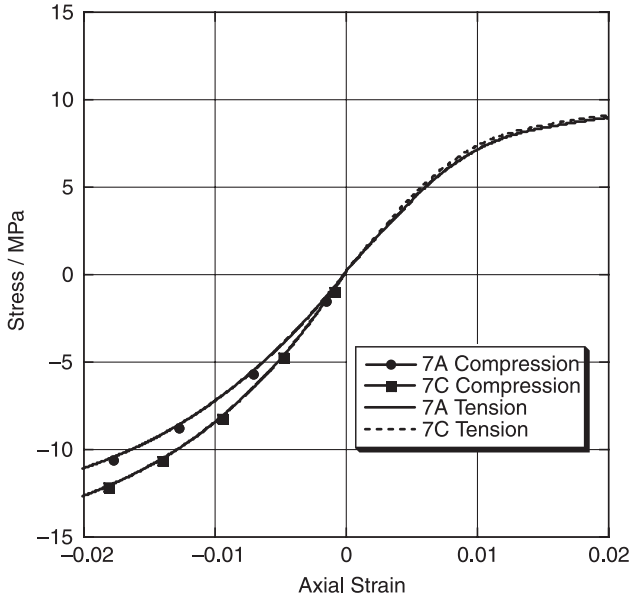

Fig. 7. Small-strain tension and compression response of 7A and 7C materials. Strain-rate $1 \times 10^{-3}\ s^{-1}$, temperature 25 ± 1 °C.

4. Results

Uniaxial tensile experiments on PTFE were undertaken at strain-rates between 2×10^{-4} and $0.1\ s^{-1}$. The results are shown in Figs. 2 and 3 for 7A and 7C materials, respectively. At first glance the strain-rate sensitivity seems relatively low in comparison to uniaxial compression [1] over the 2.5 orders of magnitude tested. However, this is an illusion caused by the immense strain to failure of Teflon. The yield stress for both materials are similar whilst the 7C Teflon has a strain to failure approximately 11% larger than 7A, leading to an ≈20% larger failure stress. Data at rates above $0.1\ s^{-1}$ could not be obtained due to the limited time response of the video extensometer.

The temperature sensitivity was measured between −50 and 150 °C and the plotted data are shown in Figs. 4 and 5. In general, the 7C Teflon failed at a slightly higher strain, however, the plots are very similar in the measured decrease in strength with increasing temperature.

As previously discussed, obtaining valid high strain-rate data for Teflon proved troublesome in the tensile Hopkinson bar. Data at three temperatures, 23, −15 and −50 °C were obtained at $800\ s^{-1}$. Fig. 6 shows the results together with a quasi-static comparison curve for material at 23 °C. Oscillation may still be observed in the high-rate data but this is an artifact of the testing method rather than reflecting a true material response. The magnitude of the oscillations is higher in the colder material reflecting less damping in the material. The assumption that, correctly time shifted, the reflected and transmitted pulses are instantaneously equal to the incident pulse is valid over the data range presented.

The video extensometer is not ideally suited to measuring small strains. For this reason strain gauges were chosen to investigate the small strain response of Teflon. Data in compression have been previously presented [1] and Fig. 7 shows this together with tensile data. It may be seen that whilst differences were noted in compression between 7C and 7A material the response was essentially identical in tension. The tensile modulus from 0.0 to 0.005% strain is approximately 860 MPa and falls midway between the plotted compressive curves for 7A and 7C. The yield is more pronounced in tension than compression and starts at approximately 1% strain.

Making use of the two axis strain gauges employed, values of Poisson ratio were calculated. This plot is shown

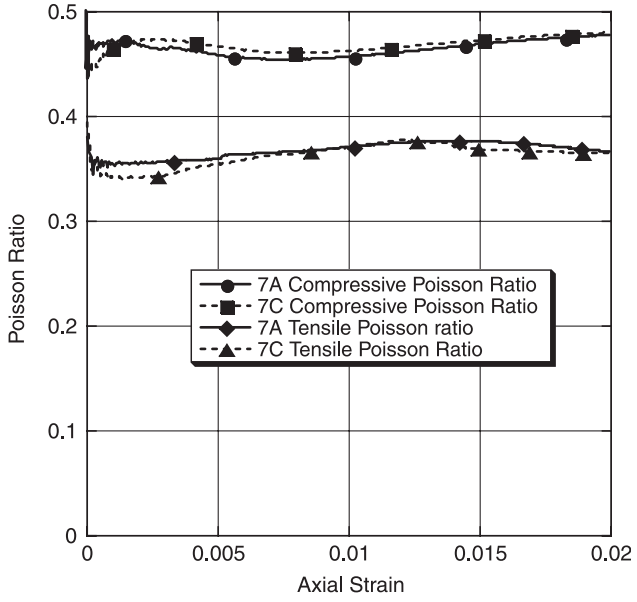

Fig. 8. Small-strain Poisson ratio calculation for 7A and 7C materials in tension and compression. Strain-rate $1\times10^{-3}\,s^{-1}$, temperature 25 ± 1 °C.

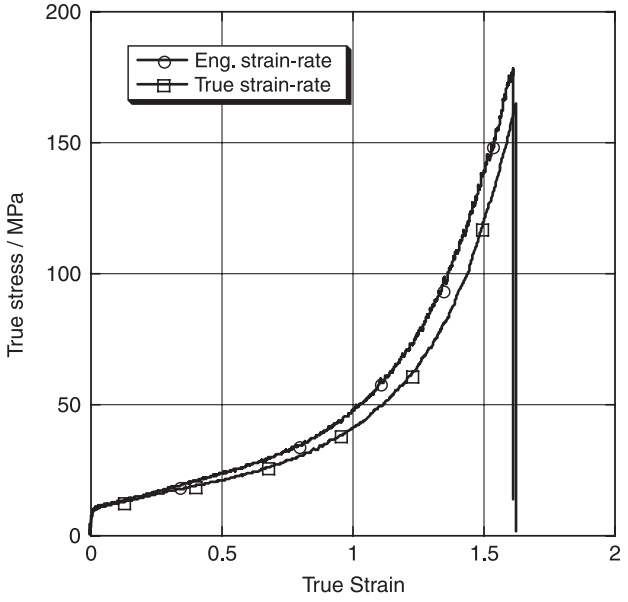

Fig. 10. Comparison of true strain-rate control vs. engineering strain-rate control. Strain-rate $5\times10^{-3}\,s^{-1}$ in each case.

in Fig. 8. It may be observed that whilst the ratio for 7A and 7C are extremely close, there is a marked difference in the tensile and compressive value. The tensile values are consistently around 0.1 lower from 0 to 2% strain.

The effects of crystallinity were investigated at 15, 23, 50 and 100 °C at a strain rate of $0.005\,s^{-1}$. Fig. 9 shows only the results for 23 and 100 °C for clarity. The behaviour is seen to be essentially identical only deviating at high temperature and high-strain. The data at 15 and 50 °C confirmed this trend. The 15 °C curves are seen to overlap and the 50 °C data shows that the lower crystallinity material is slightly stiffer at high strains.

All the large-strain experiments so far discussed were run using true strain-rate control. For comparison, an identical test was undertaken in constant engineering strain rate control (i.e. the gauge length marker speed is fixed throughout the test and related to the original gauge length of the sample). Fig. 10 shows the results of this test. Both samples exhibited similar strains to failure although in the engineering strain-rate test, the sample is stiffer at high strains.

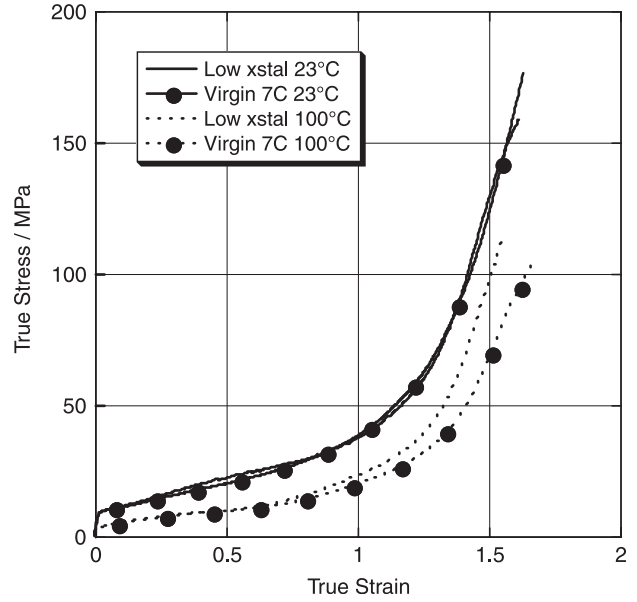

Fig. 9. The effect of crystallinity on the tensile response of PTFE at 23 and 100 °C. Low crystallinity was 28%, virgin 7C was 38% measured by MDSC. Strain-rate $1\times10^{-3}\,s^{-1}$.

5. Discussion

Owing to the high work hardening rate of PTFE retarding necking in the tensile samples, excellent reproducibility was obtained from sample to sample. In some cases up to six samples were tested under identical conditions and all the curves displayed a high degree of reproducibility. This added confidence to the data generated from difficult to machine samples, such as the Hopkinson bar geometry and limited volumes of material in the case of the reduced crystallinity tests, suggests that the smaller number of tests yielded reliable data.

As previously mentioned, the strain-rate sensitivity in tension for PTFE is actually similar to compression although it does not appear particularly significant from brief examination of the data. From close examination of Figs. 2 and 3 it may be seen that the yield stress increases by 1.7 times over 2.5 decades of strain-rate. This is more significant if one considers the Hopkinson bar high strain-rate data at room temperature. In this case the flow stress at

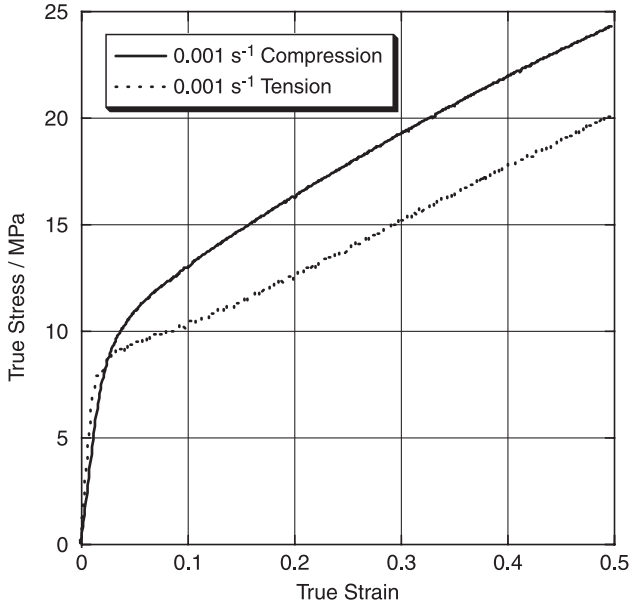

Fig. 11. A plot of tension and compression behaviour for Teflon 7C to 50% true strain. Strain-rate 5×10^{-3} s^{-1}, temperature 23 °C.

10% true strain only jumped 2.2 times for an additional strain-rate increase of 1.5×10^{5}.

The temperature effect is more evident. In this case the flow stress at 10% true strain varied by approximately 9 times from −50 to 150 °C. The samples tested at 50 °C still exhibited an overt yield point, but at 150 °C a smooth flow curve is generated with no discernable yield. While no obvious pattern is seen in the failure behaviour of the material with respect to strain-rate, a stronger dependency is observed with respect to temperature. It can be seen that the stress at failure reaches a maximum at 23 °C and drops at higher and lower temperatures while the strain to failure quickly drops at lower temperatures.

It is worth reviewing the microstructure of PTFE in an effort to understand the dependence on crystallinity. Previous studies have looked at electron micrographs of replica PTFE structures exposed by cryofracture before and after deformation at various temperatures [36]. Crystalline regions were observed, the size of which was determined by crystallinity concentrations. The crystalline regions were long narrow bands with striations parallel to the long axis. Between the crystalline regions it is supposed the amorphous regions reside. Two deformation mechanisms were identified in tension. At temperatures higher than −196 °C the amorphous regions are assumed to orientate while at the same time slip is seen to occur in the crystalline regions along the parallel striations. As slip occurs, the crystalline regions tend to orient by rotation so that the long axis is along the pulling direction. This reduces the deformation available by this mechanism. At higher strains, the crystals are observed bowing or kinking about the striations (i.e. they are no longer straight and parallel to the long axis of the crystal). Koo [21] accepted this deformation mechanism and used it to explain his observation that at low strains, higher crystallinity samples were stiffer than low, while at higher strains, more amorphous samples were stiffer. Implicit in Koo's model is the assumption that increasing the crystallinity of PTFE results in larger, not more crystalline domains. This is important because the model suggests that amorphous material is able to more fully orientate around small crystalline regions. Also, smaller crystalline regions orient more easily along the pulling axis resulting in a faster shutting down of the slip mechanism within the crystalline regions. The model therefore suggests that above cryogenic temperatures, where the amorphous regions are flexible and free to orientate upon the application of tension, the primary mode of deformation is amorphous orientation with secondary slip of the crystalline domains. This deformation mechanism allows the lower crystallinity material to flow at a lower stress than higher crystallinity. As the strain increases, little more deformation can be accommodated in the orientated amorphous regions and in low crystallinity material the slip mechanism has been exhausted owing to the long axis orientation of the crystalline regions. Therefore, at large strains lower crystallinity PTFE is stiffer that higher crystallinity material. The experiments reported on in this paper suggest that lower crystallinity material is slightly stiffer than higher at large strains, but only as the temperature is increased above room temperature. At −15 °C and room temperature no significant deviation was noted between the two crystallinities. At higher temperatures the amorphous chains are more able to orient and this may explain the results presented in this study.

The small strain tests using bonded strain gauges produced some unexpected results. Comparison between 7A and 7C material in compression revealed a difference with the 7C material being stiffer. In tension the materials are essentially identical. Additionally, the calculated Poisson ratio reveals a difference between compression and tension at small strains. Prior to testing specimens in both tension and compression samples were machined from both in-plane and through-thickness directions of the billet. It was discovered that the compression results depended slightly on the direction (an approximately 5% higher value was measured in yield stress between the through thickness and in-plane direction) and so all the compression samples were cut from the in-plane direction [1]. A slight billet 'skin' effect was also noted in compression and so samples were not machined from material within 10 mm of the faces. In tensile tests, no significant difference in yield or failure stress or strain to failure could be detected irrespective of orientation. Despite this, the data for all samples reported here came from through-thickness specimens. The change in response at small strains and in orientation effects suggests a difference in deformation mechanism between compression and tension. This observation is substantiated by plotting compression and tension data at 1×10^{-3} s^{-1} on the same axis and is shown in Fig. 11. A more pronounced

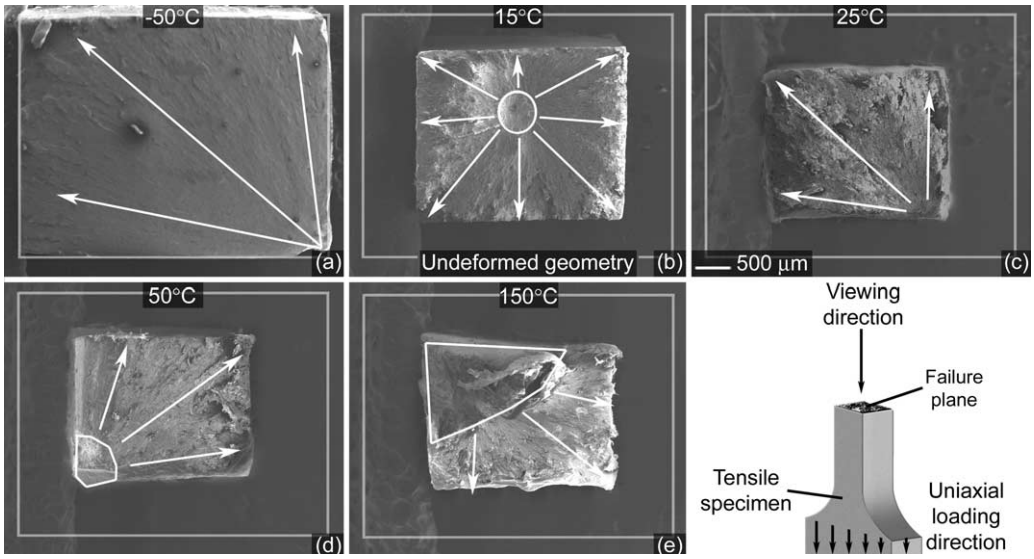

Fig. 12. Temperature sensitivity of 7C material failure mechanisms. The initial undeformed geometries are indicated by the grey boundaries. Failure propagation paths are indicated with white arrows. The white boundaries in (b), (d), and (e) highlight regions of fibril formation. Strain-rate $5\times10^{-3}\ s^{-1}$.

yield occurs in tension, however, the material in both states work hardens at approximately the same rate. An obvious explanation for this tension vs. compression behaviour does not present itself, but in semi-crystalline polymers various modes of deformation are available such as void formation followed by micro-fibril growth, crystalline slip, twinning and various lamellar deformation modes. Some or all of these can be excited or retarded depending on whether the local stress state is positive or negative [42].

Considerable heating occurs as large tensile strains are imposed on PTFE. This presents an obvious possible explanation for the engineering strain-rate test appearing stiffer than the true rate one. The cross-head speed is increasing in true strain-rate control as the specimen increases in length generating more heat per unit time than a test run at constant engineering rate. It may, therefore, be that thermal softening results in the softer response of the 'faster' test, despite the nominal increase in apparent strain-rate. This hypothesis differs from the work done in compression by Chou et al. [43] who suggested that at strain rates below approximately $1\ s^{-1}$ samples remained isothermal. It should be noted that Chou's data were in compression to true strains of only 20% unlike this tensile data to strains of ca. 1.6. Unfortunately, it has not yet been possible to accurately measure the temperature rise of samples in tension, however, upon removal from the grips after fracture the samples were noticeably warmer than room temperature. Therefore, in quasi-static large strain tension the samples were obviously neither isothermal or adiabatic.

Fig. 12 shows representative failure surfaces at −50, 15, 25, 50, and 150 °C. The initial undeformed geometries are indicated in each frame, as a point of reference to the final

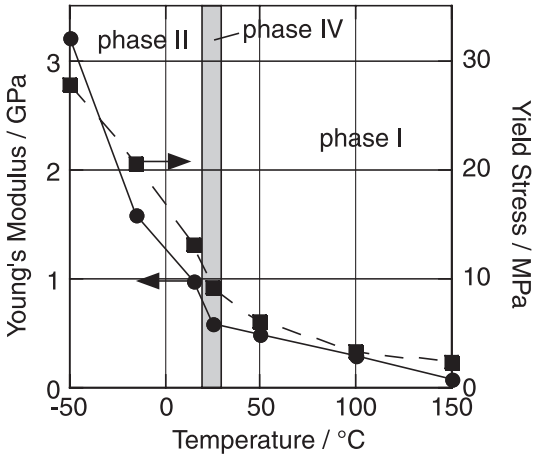

Fig. 13. Young's modulus and 2% offset yield stress of PTFE 7C as a function of temperature. Strain-rate $5\times10^{-3}\ s^{-1}$.

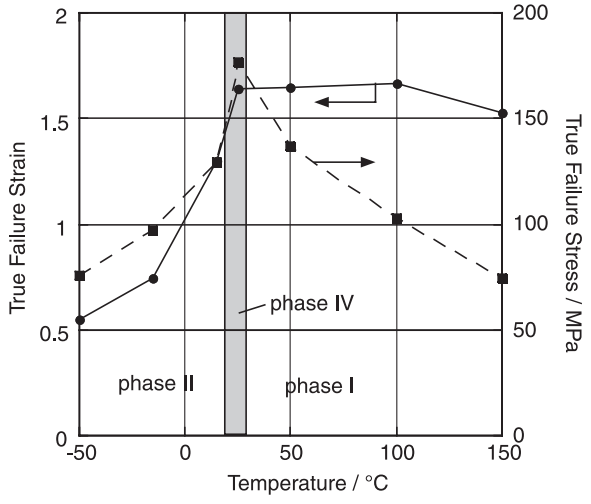

Fig. 14. True strain to failure and true failure stress of PTFE 7C as a function of temperature. Strain-rate $5\times10^{-3}\ s^{-1}$.

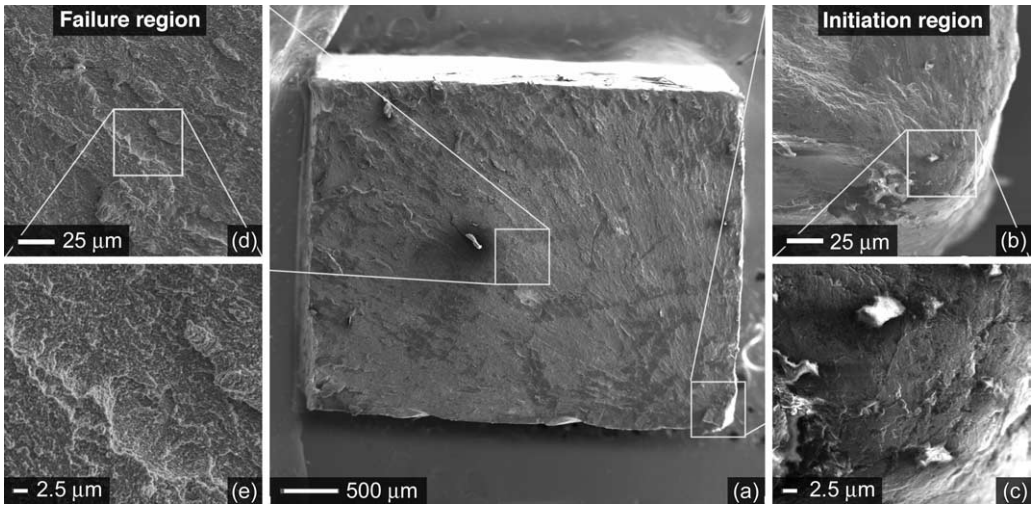

Fig. 15. Crack initiation and propagation in 7C material at −50 °C in phase II. Strain-rate $5\times10^{-3}\,s^{-1}$.

deformed cross section. Despite significant plastic deformation and a corresponding reduction in cross sectional area, PTFE resists localized necking and instead draws uniformly through the gage length of the tensile samples. This enables extension to high strains, with substantial strain hardening. In each case failure occurred perpendicular to the loading direction, with no sign of shear lip formation or other signs of a highly triaxial stress state associated with failure. The location of failure initiation and the crack path are indicated for the different temperatures. In addition to the reduction in yield stress and Young's modulus observed with increased temperature (Fig. 13), the failure behavior is strongly temperature dependent, as shown in Fig. 14. From −50 to 25 °C the true strain to failure increases three fold and the true failure stress more than doubles. From 25 to 150 °C, a second behavior regime is observed with a nominal change in the true strain to failure, while the true failure stress decreases by one half.

As discussed at length by Brown and Dattelbaum [39], PTFE is a semi-crystalline polymer with four distinct temperature and pressure dependent crystalline phases, with three of the crystalline structures observed at ambient pressure. The first-order transition at 19 °C between phases II and IV is an unraveling in the helical conformation. Further rotational disordering and untwisting of the helices occurs above 30 °C giving way to phase I. The range of temperatures investigated encompasses the three ambient pressure phases with transitions at 19 and 30 °C [22]. The reported transition temperatures correspond to the maxima points of the heat flow measured by differential scanning calorimetry (DSC), but the thermodynamically pure crystalline structures for PTFE in phases II and I, only exist below 0 °C and above 35 °C, respectively [39]. Therefore, the temperature range investigated encompasses four ambient pressure phase conditions: −50 and −15 °C are PTFE in phase II, 15 °C is PTFE in the transition from phase II to phase IV, 25 °C is PTFE in phase IV, and 50, 100 and 150 °C are PTFE in phase I. As shown in Fig. 14, the

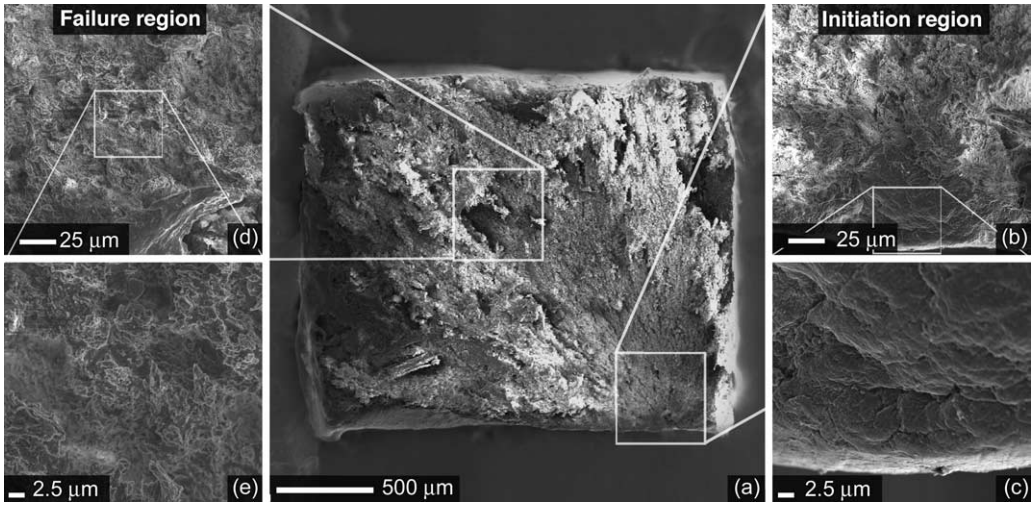

Fig. 16. Crack initiation and propagation in 7C material at 25 °C in phase IV. Strain-rate $5\times10^{-3}\,s^{-1}$.

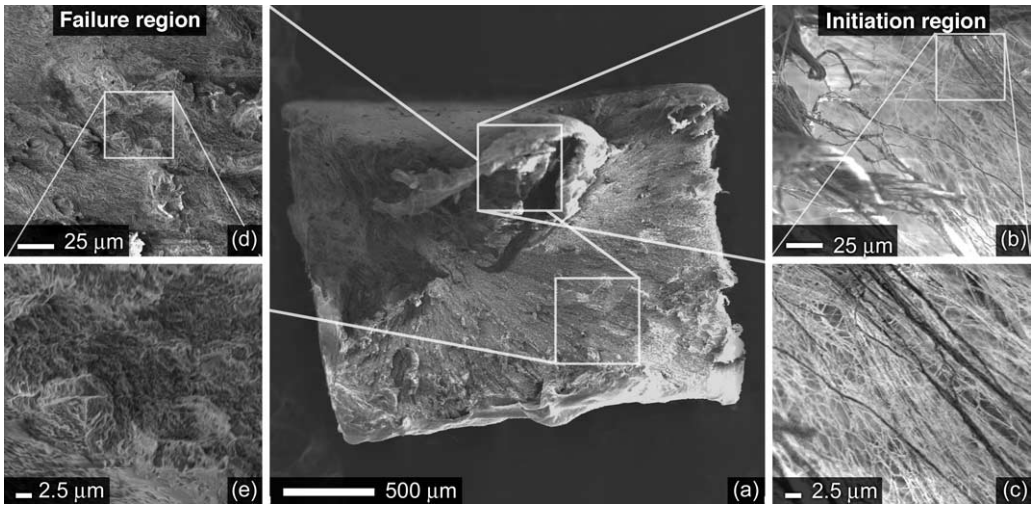

Fig. 17. Crack initiation and propagation in 7C material at 150 °C in phase I. Strain-rate 5×10^{-3} s^{-1}.

observed transition in the temperature dependence of the failure behavior corresponds exactly with the crystalline phase transitions from phase II, through phase IV, and into phase I. To a lesser degree, the temperature dependence of the Young's modulus and yield stress both appear to be bimodal, with a steeper slope below room temperature for PTFE in phase II and a second shallower slope above room temperature for PTFE in phase I. The connection of mechanisms for tensile deformation and failure to crystalline phase structure is supported by early work by Wecker et al. [44] showing a dependence of crystal orientation under load on crystalline phase.

To understanding the dependence of failure on temperature, it is essential to examine mechanisms of failure as elucidated by the evolved microstructure. Polytetrafluoroethylene in phase II, as represented at −50 °C in Fig. 15, exhibits little plastic deformation and a brittle failure morphology. Failure is initiated at a corner (Fig. 15(a)–(c)) and propagates radially through the material as indicated by faint river markings on the surface (Fig. 15(a)). Under higher magnification (Fig. 15(d) and (e)) evidence of microvoid coalescence is observed. The length scales associated with this morphology are an order of magnitude smaller than the PTFE 7C molding powder (average length ≈ 20 μm). At room temperature PTFE in phase IV exhibits signs of substantial plastic deformation, both in the reduction in cross sectional area (Fig. 12(c)) and failure morphology (Fig. 16). Similar to PTFE in phase II, failure of PTFE in phase IV is initiated near a corner (Fig. 16(a) and (c)), with a relatively brittle morphology at the initiation point. However, the material exhibits significant localized plastic deformation, imparting a stable porous microstructure capable of carrying high stress and strain (Fig. 16(d) and (e)). Through the gauge length where the PTFE has undergone plastic deformation, stress whitening is observed suggesting the formation of a microstructure throughout the material, and not just limited to the failure surface. Polytetrafluoroethylene in phase I, as

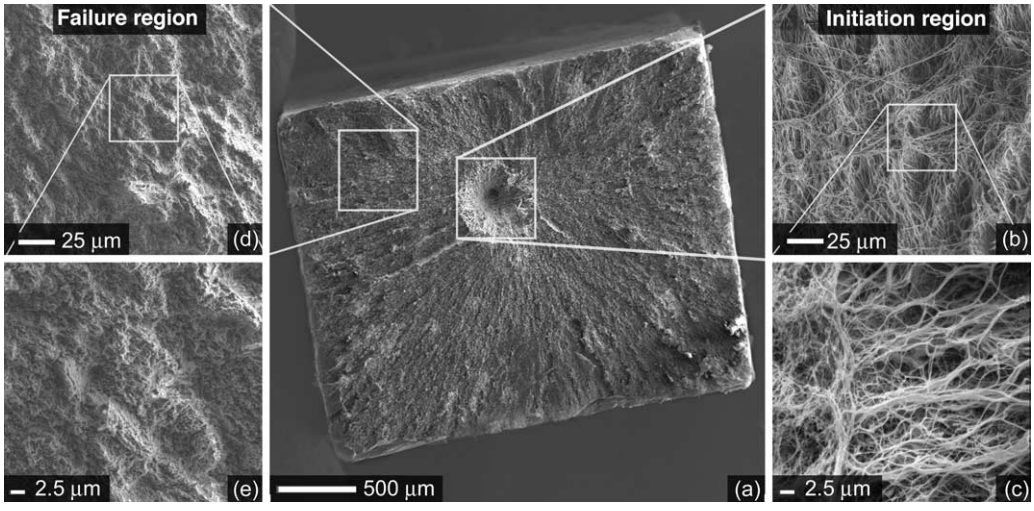

Fig. 18. Crack initiation and propagation in 7C material at 15 °C in the transition from phase II to phase IV. Strain-rate 5×10^{-3} s^{-1}.

represented at 150 °C in Fig. 17, exhibits similar levels of plastic deformation as indicated by cross sectional area and stress whitening to PTFE in phase IV. Failure is initiated at a corner (Fig. 17(a) and (c)) but two distinct mechanisms of plastic deformation are observed. In the region of crack growth (Fig. 17(d) and (e)), a porous microstructure very similar to PTFE in phase IV is observed. In the region of crack initiation, however, a dense network of polymer fibrils is formed (Fig. 17(b) and (c)). The region of fibril formation increases with temperature, as shown in Fig. 12(d) and (e). The formation of fibrils provides an effective mechanism to dissipate energy, but also serves to orient the polymer providing increases in strength and stiffness. A detailed discussion of PTFE fibril formation and structure is presented by Brown and Dattelbaum [39].

The only condition under which failure did not originate at a corner of the sample was at 15 °C, the test performed in the transition form a phase II crystalline structure to phase IV (Fig. 18). In this case, failure initiated in the centre of the specimen (Fig. 12(b)) with the formation of stable fibrils (Fig. 18(b) and (c)) followed by radial brittle failure indicative of PTFE in phase II (Fig. 18(d) and (e)). The combination of failure modes may result in part from the transition structure of crystalline domains. Moreover, internal friction during loading results in a temperature rise in the specimen that could lead to further transformation of the crystalline structure. Since the temperature rise is the highest in the centre of the specimen, the centre could be in phase IV, while the surrounding material is in the transition from phase II to phase IV.

6. Conclusions

In conclusion, in this study the mechanical properties of PTFE in tension were found to be sensitive to strain-rate and temperature and to a smaller extent crystallinity. Slight differences were found between Teflon 7A and 7C material, but in all cases the same trends were exhibited. The Poisson ratio was measured and found to be different in tension and compression. A definitive explanation for this response is still required but it is postulated to be due to a difference in deformation mechanism between tension and compression.

Acknowledgements

The authors wish to thank Dr Dana Dattelbaum, Dr Bruce Orler and Dr George T. (Rusty) Gray (LANL) for useful discussions regarding this research. Carl Trujillo is thanked for help with the tensile Hopkinson bar experiments. This project was supported under the auspices of the US Department of Energy, specifically in part by the joint DoD/DoE Munitions Technology Development Program. Electron microscopy was performed in the Electron Microscopy Laboratory at LANL with the assistance of R. Dickerson. E.N. Brown acknowledges the Los Alamos National Laboratory Directors Funded Postdoctoral Fellowship program for support.

References

[1] Rae P, Dattelbaum D. The properties of poly(tetrafluoroethylene) (PTFE) in compression. Polymer 2004;45:7615–25.
[2] Renfrew MM, Lewis EE. Polytetrafluoroethylene; heat-resistant, chemically inert plastic. Ind Eng Chem 1946;38(9):870–7.
[3] Doban RC, Sperati CA, Sandt BW. The physical properties of 'teflon', polytetrafluoroethylene. Soc Plast J 1955;11:17–21 [see also p. 24 and 30].
[4] Thomas PE, Londz JF, Sperati CA, McPherson JL. Effects on fabrication on the properties of teflon resins. Soc Plast J 1956;12: 89–95.
[5] Joyce J. Fracture toughness evaluation of polytetrafluoroethylene. Polym Eng Sci 2003;43:1702–14.
[6] Fischer S, Brown N. Deformation of polytetrafluoroethylene from 78 to 298 k and the effect of environmental crazing. J Appl Phys 1973; 44(10):4322–7.
[7] Brown N, Parrish M. Effect of liquid nitrogen on the tensile strength of polyethylene and polytetrafluoroethylene. J Polym Sci, Polym Lett Ed 1972;10:777–9.
[8] Sauer JA, Pae K. Flow of solid polymers under high pressure. Colloid Polym Sci 1974;252:680–95.
[9] Zerilli FJ, Armstrong RW. Thermal activation constituative model for polymers applied to polytetrafluoroethylene. In: Furnish MD, Thadhani NN, Horie Y, editors. AIP conference proceedings: Shock compression of condensed matter-2001, vol. 620. Melville, NY: American Institute of Physics; 2001. p. 657–60.
[10] Tervoort T, Visjager J, Graf B, Smith P. Melt-processable poly(tetrafluoroethylene). Macromolecules 2000;33:6460–5.
[11] Kletschkowski T, Schomburg U, Katsumura Y. Endochronic viscoplastic material models for filled PTFE. Mech Mater 2002;34: 795–808.
[12] Wall L, Florin R. Polytetrafluoroethylene—a radiation-resistant polymer. J Appl Polym Sci 1959;II(5):251.
[13] Kudoh H, Sasuga T, Seguchi T, Katsumura Y. High energy ion irradiation effects on polymer material: 4 heavier ion irradiation effects on mechanical properties of PE and PTFE. Polym Commun 1996;37:3737–9.
[14] Fayolle B, Audouin L, Verdu J. Radiation induced embrittlement of PTFE. Polymer 2003;44:2773–80.
[15] Peng G, Geng H, Yang D, He S. An analysis on changes in structure, tensile properties of polytetrafluoroethylene film by protons. Radiat Phys Chem 2004;69:163–9.
[16] Nishioka A, Watanabe M. Viscosity and elasticity of polytetrafluoroethylene resin above the melting point. J Polym Sci 1957;24(106): 298–300.
[17] Dyment J, Ziebland H. The tensile properties of some plastics at low temperatures. J Appl Chem 1958;8:203–6.
[18] DuPont-fluoroproducts, Teflon, PTFE, properties handbook. Tech. Rep. H-37051-3, DuPont; 1996.
[19] Koo GP, Jones ED, Riddell MN, O'Toole JL. Engineering properties of a new polytetrafluoroethylene. Soc Plast J 1965;21(9):1100–5.
[20] Koo GP, Andrews RD. Mechanical behavior of polytetrafluoroethylene around the room-temperature first-order transition. Polym Eng Sci 1969;9(4):268–76.
[21] Koo GP. Cold drawing behavior of polytetrafluoroethylene PhD reprinted by Unversity Microfilms Inc. Ann Arbor, Michigan, USA: Sc.d, Stevens Institute for Technology; 1969.
[22] Sperati CA, Starkweather HW. Fluorine-containing polymers. Part II. Polytetrafluoroethylene. Adv Polym Sci 1961;2:465–95.

[23] McCrum NG. An internal friction study of polytetrafluoroethylene. J Polym Sci 1959;34:355–69.
[24] Wilson CW, Pake GE. Nuclear magnetic resonance determination of degree of crystallinity in two polymers. J Polym Sci 1953;10(5): 503–5.
[25] Moynihan RE. Infrared studies on polytetrafluoroethylene. Meeting of the American Chemical Society, Atlantic city 1956. p. 9S.
[26] McCrum NG. Torsion pendulum method for determining crystallinity and void content of tetrafluoroethylene resins. ASTM Bull 1959;242: 80–2.
[27] Lehnert RJ, Hendra PJ, Everall N, Clayden NJ. Comparative quantitative study on the crystallinity of poly(tetrafluoroethylene) including Raman, infrared and ^{19}F nuclear magnetic resonance spectroscopy. Polymer 1997;38(7):1521–35.
[28] Berry KL, Peterson JH. Tracer studies of oxidation–reduction polymerization and molecular weight of 'teflon' tetrafluoroethylene resin. J Am Chem Soc 1951;73:5195–7.
[29] Doban RC, Knight AC, Peterson JH, Sperati CA. Molecular weight of polytetrafluoroethylene. Meeting of the American Chemical Society, Atlantic city 1956 p. 9S.
[30] Suwa T, Seguchi T, Takehisa M, Machi S. Effect of molecular weight on the crystalline structure of polytetrafluoroethylene as-polymerized. J Polym Sci, Polym Lett Ed 1975;13:2183–94.
[31] Rigby HA, Bunn CW. A room-temperature transition in polytetrafluoroethylene. Nature 1949;164:583.
[32] Bunn CW, Cobbold AJ, Palmer RP. The fine structure of polytetrafluoroethylene. J Polym Sci 1958;28:365–76.
[33] Clark ES, Muus LT. The relationship between Bragg reflections and disorder in crystalline polymers. Zeitschrift fur Kristallographie 1962; 117:108–18.
[34] Clark ES, Muus LT. Partial disordering and crystal transitions in polytetrafluoroethylene. Zeitschrift fur Kristallographie 1962;117: 119–27.
[35] Pierce RHH, Clark ES, Whittney JF, Bryant WMD. Crystal structure of polytetrafluoroethylene. Meeting of the American Chemical Society, Atlantic city 1956.
[36] Speerschneider CJ, Li CH. A correlation of mechanical properties and microstructure of polytetrafluoroethylene at various temperatures. J Appl Phys 1963;34:3004–7.
[37] Weeks JJ, Clark ES, Eby RK. Crystal structure of the low temperature phase (ii) of polytetrafluoroethylene. Polymer 1981;22:1480–6.
[38] Eby RK, Clark ES, Farmer BL, Piermarini GJ, Block S. Crystal structure of poly(tetrafluoroethylene) homo- and copolymers in the high pressure phase. Polymer 1990;31:2227–37.
[39] Brown E, Dattelbaum D. The role of crystalline phase on fracture and microstructure evolution of polytetrafluoroethylene. Polymer 2005; 46:3056–68.
[40] Nemat-Nasser S, Isaacs J, Starrett J. Hopkinson techniques for dynamic recovery experiments. Proc R Soc London, Ser A 1991;435: 371–91.
[41] Gray III GT. Classic split-Hopkinson pressure bar testing. In: Kuhn H, Medlin D, editors. ASM handbook. vol. 8. Ohio: ASM International; 2000. p. 462–73.
[42] Galeski A. Strength and toughness of crystalline polymer systems. Prog Polym Sci 2003;28:1643–99.
[43] Chou S, Robertson K, Rainey J. The effect of strain rate and heat developed during deformation on the stress–strain curve of plastics. Exp Mech 1973;13:422–32.
[44] Wecker S, Davidson T, Baker D. Preferred orientation of crystallites in uniaxially deformed polytetrafluoroethylene. J Appl Phys 1972;43: 4344–8.